J Mater Sci (2009) 44:74–83
DOI 10.1007/s10853-008-3122-z

Effect of Zn concentration on the microstructures and mechanical properties of extruded Mg–7Y–4Gd–0.4Zr alloys

Ke Liu · Jinghuai Zhang · Wei Sun · Xin Qiu · Huayi Lu · Dingxiang Tang · L. L. Rokhlin · F. M. Elkin · Jian Meng

Received: 24 September 2008 / Accepted: 17 November 2008 / Published online: 11 December 2008

Abstract Microstructures and mechanical properties of the Mg–7Y–4Gd–*x*Zn–0.4Zr ($x = 0.5$, 1.5, 3, and 5 wt.%) alloys in the as-cast, as-extruded, and peak-aged conditions have been investigated by using optical microscopy, scanning electron microscope, X-ray diffraction, and transmission electron microscopy. It is found that the peak-aged Mg–7Y–4Gd–1.5Zn–0.4Zr alloys have the highest strength after aging at 220 °C. The highest ultimate tensile strength and yield tensile strength are 418 and 320 MPa, respectively. The addition of 1.5 wt.% Zn to the based alloys results in a greater aging effect and better mechanical properties at both room and elevated temperatures. The improved mechanical properties are mainly ascribed to both a fine β' phase and a long periodic stacking-ordered structure, which coexist together in the peak-aged alloys.

K. Liu · J. Zhang · W. Sun · X. Qiu · H. Lu · D. Tang · J. Meng (✉)
State Key Laboratory of Rare Earth Resources Utilization, Changchun Institute of Applied Chemistry, Chinese Academy of Sciences, Changchun 130022, People's Republic of China
e-mail: jmeng@ciac.jl.cn

K. Liu · J. Zhang
Graduate School of the Chinese Academy of Science, Beijing 100049, China
e-mail: keliu@ciac.jl.cn

L. L. Rokhlin · F. M. Elkin
Baikov Institute of Metallurgy and Materials Science, Russian Academy of Sciences, Moscow, Russia

Introduction

As the lightest metallic structural materials, magnesium alloys have drawn great attention recently. However, the mechanical properties of magnesium alloys, both in the cast and wrought conditions, are most inferior [1], especially at high temperature. To the best of our knowledge, the addition of the rare-earth (RE) elements to magnesium alloys improves creep properties, e.g., WE54 commercial alloy [2].

Magnesium alloys containing RE alloying additions show good precipitation hardening during the peak aging process [3, 4]. Zn is often added to further improve the mechanical properties by both solid solution strengthening and age hardening [5, 6]. Nie et al. [7] reported that the addition of Zn to the Mg–6Gd–0.6Zr alloys could improve the mechanical and creep properties. The notable improvement in mechanical properties can be contributed to a dense and uniform distribution of the Mg_5Gd phase [8]. In addition, Yamasaki et al. [9] have developed a hot-extruded Mg–2.3Zn–14Gd (wt.%) alloy which displays a highest tensile proof strength of 345 MPa and a better elongation of 6.3%, due to the precipitation of a coherent 14H long periodic stacking-ordered structure precipitate shaped from the supersaturated α-Mg matrix.

It is known that Mg–Gd–Y alloys exhibit a three-stage precipitation sequence during aging at 200 °C, α'-Mg (S.S.S.S) → β'' (DO_{19}) → β' (cbco) → β (fcc) [10, 11]. Furthermore, a four-stage precipitation sequence in Mg–Gd, Mg–Gd–Nd, and Mg–Dy–Nd alloys has also been observed during aging at 250 and 300 °C [12, 13]. The sequence consists of α'-Mg (S.S.S.S) → β'' (DO_{19}) → β' (cbco) → β_1 (fcc) → β (fcc). However, it is the β' phase, with a cbco structure, distributed throughout the α-Mg matrix that contributes most to the age hardening response [3, 4, 14].

Considering the interaction of the Zn and RE elements, Yamada et al. [15] improved on the Mg–2.1Gd–0.6Y–0.2Zr alloys by the addition of Zn, which leads to improve mechanical properties. In this article, Mg–7Y–4Gd–*x*Zn–0.4Zr ($x = 0.5$, 1.5, 3, and 5) alloys were produced using the method of water-cooled iron mold casting ingot processing. The phase compositions, aging hardening behavior, microstructures and mechanical properties at both room and elevated temperatures have been investigated.

Experimental procedures

The alloy ingots with nominal compositions of Mg–7Y–4Gd–*x*Zn–0.4Zr ($x = 0.5$, 1.5, 3, and 5 and are indentified as A, B, C, and D, respectively) were melted from high-purity Mg (99.5%), high-purity Zn (>99.9%), Mg–20Y (wt.%), Mg–25Gd (wt.%), and Mg–35Zr (wt.%) master alloys. Melting was conducted in an electric resistance furnace at about 750 °C being companied with the protective atmosphere composed of CO_2 and SF_6 with the ratio of 99:1 in a mild steel crucible. At 730 °C, the melts were poured into a water-cooled iron mold with an ingot diameter of 90 mm. Specimens used for as-cast research were cut from these cylindrical ingots. Parts of them were machined into rectangular tensile specimens of 15 mm in gauge length, 3 mm in width, and 1.5 mm in thickness, and the remaining was used for other investigations. The cylindrical ingots were homogenized at 500 °C for 10 h, milled into a diameter of 82 mm, and then were extruded into rods with a diameter of 20 mm with an extrusion ratio of about 17 at 410 °C. Some rods were directly aged at 220 °C in order to investigate the age hardening behavior with time. The tensile specimens of the as-extruded and peak-aged alloys were also machined into the same geometry as the as-cast samples.

Tensile tests were carried out on a uniaxial tensile testing machine equipped with a heating chamber at a speed of 1 mm/min. The tensile axis was aligned parallel to the extrusion direction. Vickers hardness was measured by FM-700 hardness tester with a load of 300 g, a dwelling time of 15 s and 20 measurements were collected for each sample. The microstructures of the alloys were observed by an Olympus GX71 optical microscopy (OM), scanning electron microscopy (SEM) with energy dispersive spectroscopy (EDS), and transmission electron microscopy (TEM). The grain size of the alloys was measured by using an average linear intercept method. The samples were mechanically polished and then etched in a solution of 4 mL nitric acid and 96 mL ethanol. Samples for TEM were prepared by a twin-jet technique. Phase analysis was conducted by X-ray diffraction (XRD).

Experimental results

Microstructures of as-cast alloys

Figure 1 shows the microstructures of the as-cast alloys A, B, C, and D using OM (Fig. 1a, c, e, and g) and SEM (Fig. 1b, d, f, and h), respectively. The as-cast alloys are composed of dendrites of α-Mg and amounts of eutectics existing at the triple points of the grains, as shown in Fig. 1a, c, e and g. These eutectics are distributed along the grain boundaries discontinuously. Images at higher magnification of the as-cast alloys were obtained by the SEM. It is observed that a lamellar phase appears at the grain boundaries in all four alloys, as shown in Fig. 1b, d, f, and h. The SEM observations clearly show the presence of the lamellar phase along the grain boundaries, and the volume fraction of this phase increases with increasing the content of Zn.

Figure 2 shows the XRD patterns obtained for the as-cast alloys. It can be observed that the as-cast alloys are mainly composed of a α-Mg solid solution together with $Mg_{24}(Y, Gd)_5$, $Mg_5(Y, Gd)$, and $Mg_{12}Zn(Y, Gd)$ secondary phases where Gd probably substitutes for Y. As seen in Fig. 2, the peaks of the $Mg_{12}Zn(Y, Gd)$ phase are strengthened with increasing the amount of Zn addition. The $Mg_{12}ZnY$ phase in Mg–Zn–Y alloy was first reported by Padezhnova et al. [16], and the microstructure of this phase was introduced by Luo [17]. The 18R long period ordered stacking structural $Mg_{12}ZnY$ (Z-phase) forms in Mg–Zn–Y alloys via rapid solidification, because increasing the cooling rate and adding Y can reduce the energy barrier for forming the Z-phase [18, 19]. It has been reported that long period-ordered stacking structural precipitates also occur in rapidly solidified Mg–Zn–Dy, Mg–Zn–Ho, and Mg–Zn–Er alloys as well as in the Mg–Zn–Y alloy system [20].

Figure 3 shows SEM images and corresponding EDS results of the as-cast alloy B. The EDS suggests that the composition of the lamellar phase is Mg–6.24 at.%Y–1.79 at.%Gd–4.24 at.% Zn, as shown in Fig. 3c. The concentrations are similar to those in the 18R LPS phase reported by Itoi et al. [21]. Moreover, the formation of LPS structures occurs through a diffusion-controlled process [22]. The lamellar phase in all the as-cast alloys A, B, C, and D can be considered to be the $Mg_{12}Zn(Y, Gd)$ phase with the 18R LPS morphology. Figure 3d shows the EDS analysis result from point B as indicated in Fig. 3b. The result suggests that the composition of the square particle is Mg–16.60 at.%Y–4.25 at.%Gd–2.17 at.% Zn. This chemical composition is close to $Mg_5(Y, Gd)$ without considering about the content of Zn in the EDS result.

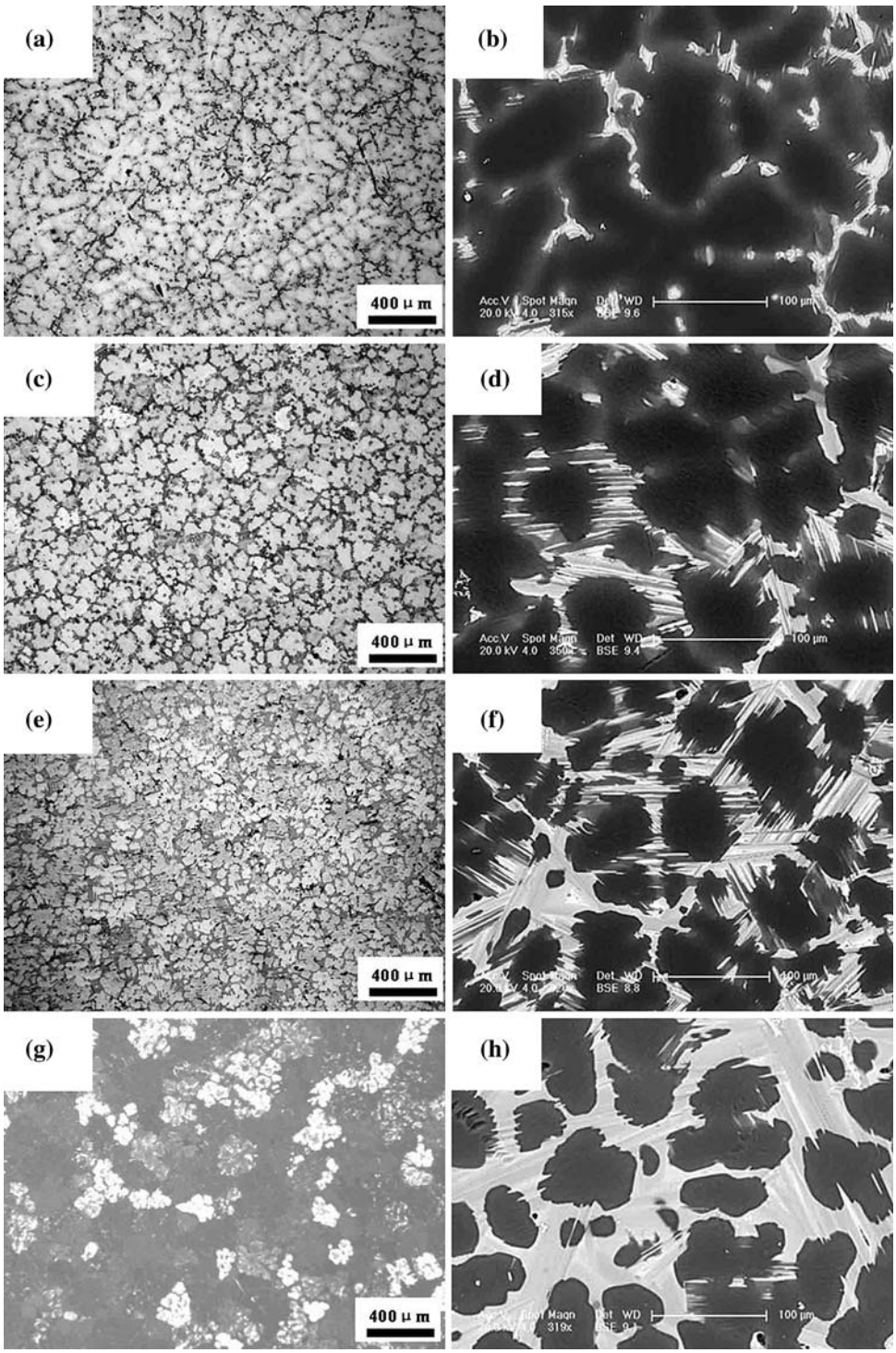

Fig. 1 Optical and SEM images of the as-cast alloys: **a**, **b** alloy A; **c**, **d** alloy B; **e**, **f** alloy C; **g**, **h** alloy D

Microstructures of as-extruded alloys

Figure 4 shows the optical micrographs of the hot-extruded alloys. Both the dendrites of α-Mg and Coarse $Mg_{12}Zn$(Y, Gd) intermetallics were crushed during hot extrusion. These intermetallics are distributed along the extrusion direction, as shown in Fig. 4. The average grain size of the hot-extruded alloy A is about 12 μm. It is observed that a few of the intermetallics are located at grain boundaries in the alloy A. The hot-extruded alloy B has smaller grain size compared with the hot-extruded alloy A, i.e., about 11 μm. Lots of intermetallics are found at the grain boundaries in this alloy. The average grain size of the alloy C after hot extrusion is probably 10 μm. Grain size of the alloy D is

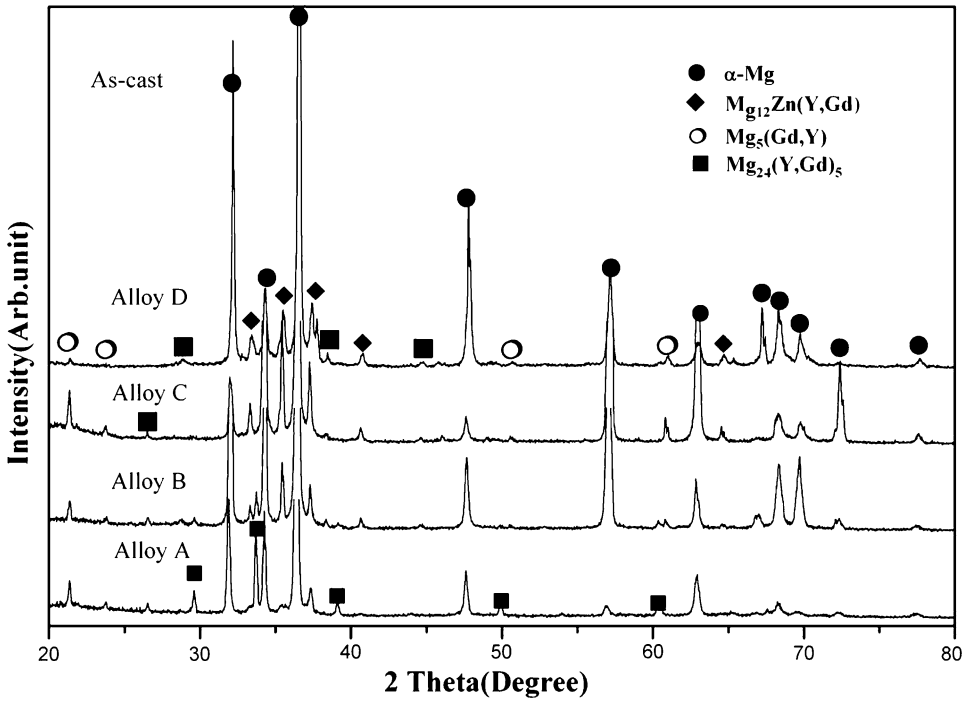

Fig. 2 XRD patterns of the as-cast alloys A, B, C, and D

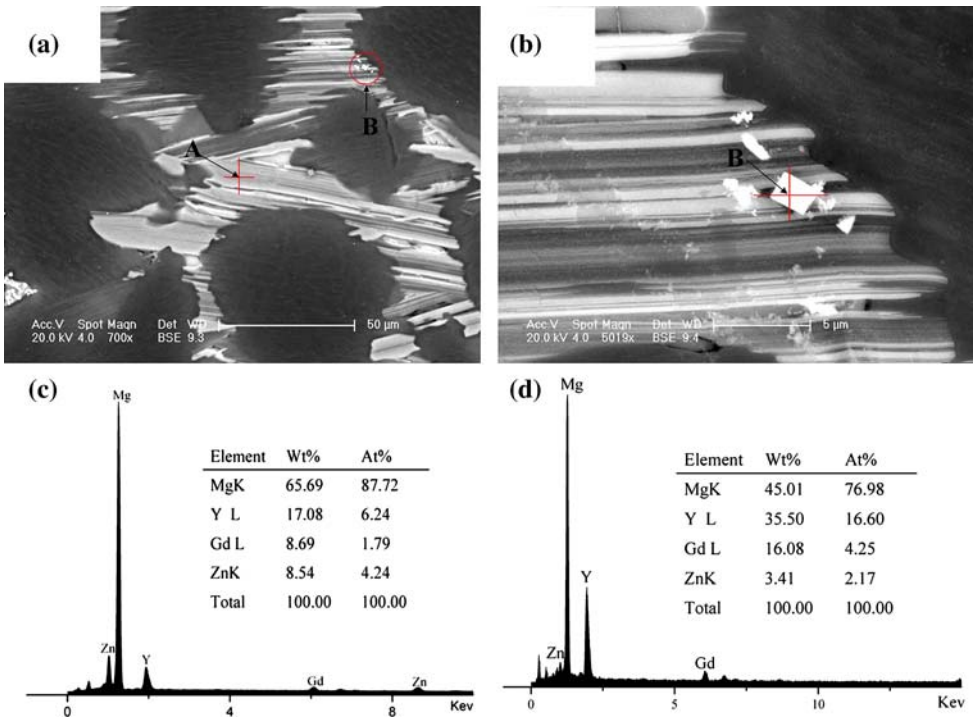

Fig. 3 SEM images and EDS results of the as-cast alloy B: **a** SEM micrograph; **b** large magnification of the cubic precipitate corresponding to the point B; **c**, **d** EDS results of the points A and B, respectively

smallest in all of them, i.e., about 9.5 μm. Moreover, more big chunks of intermetallics are located at grain boundaries in the as-extruded alloys C and D.

As stated above, the microstructures of all four alloys after hot extrusion are refined. Figure 4 shows that dynamic recrystallization (DRX) occurred in alloys during hot extrusion. The refined microstructure is ascribed to this DRX [23–25]. It has been reported that dislocations accumulate together with high density at both coarse grain boundaries and secondary particles to produce cells separated by dislocation walls, and these walls convert to subgrain structures by a subsequent recovery process [24, 25]. The subgrain structures will form over the whole volume of the grain via the conversion of dislocation cell walls into subgrain boundaries.

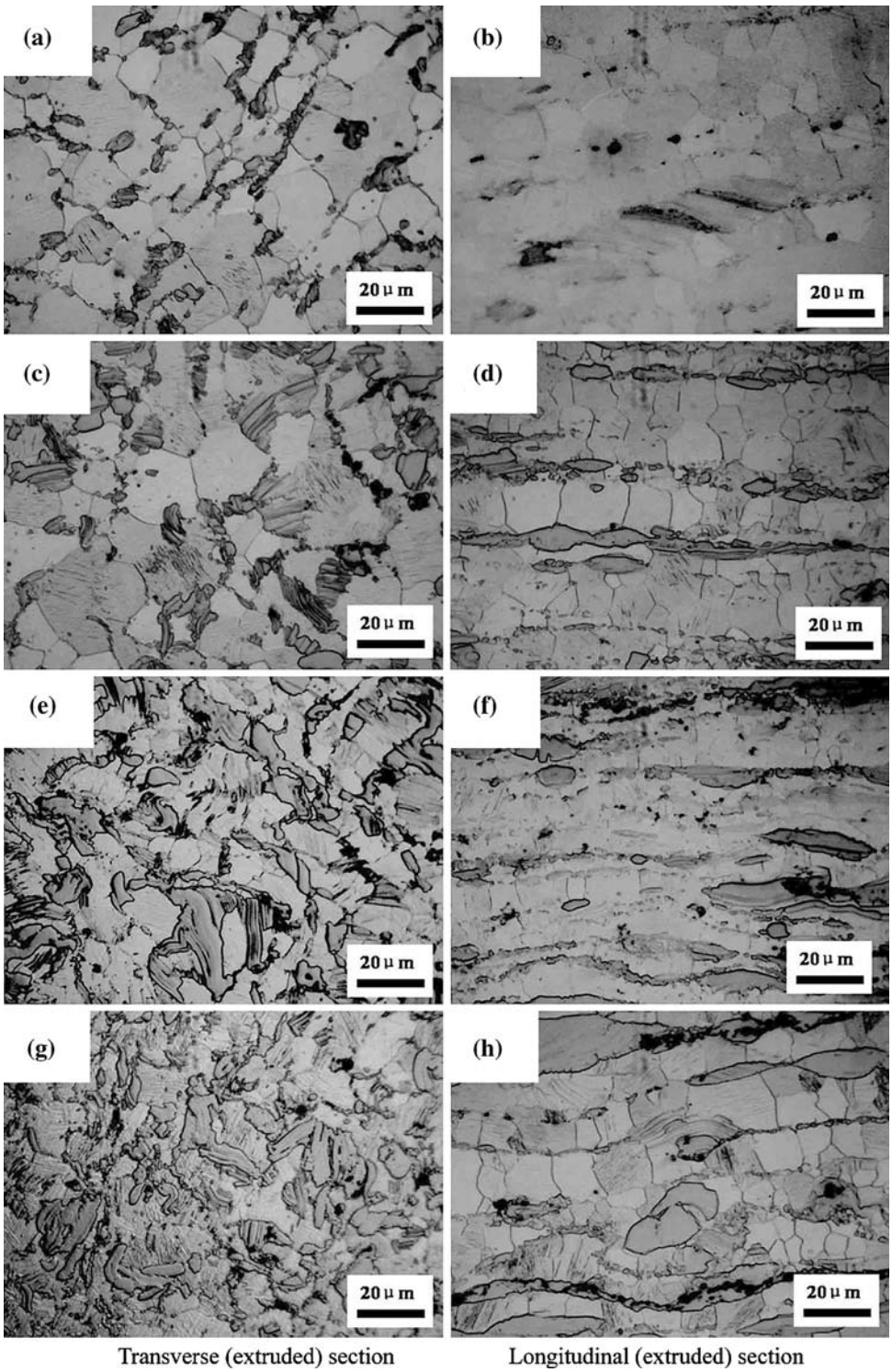

Fig. 4 Optical images of the as-extruded alloys: **a**, **b** alloy A; **c**, **d** alloy B; **e**, **f** alloy C; **g**, **h** alloy D

Figure 5 shows images of a specimen of alloy B via compression deformation at 410 °C, a speed of 1 mm/min, in order to investigate the DRX mechanism. Before compression test, this specimen was treated with solid solution at 500 °C for 10 h, and then quenched into warm water. Figure 5a shows the OM image of the deformation specimen. Both grains and Z-phase are elongated along the deformation direction, and DRX occurred. Recrystallized grains formed and distributed at an interface between matrix and Z-phase (see Fig. 5a). It is found that dislocations accumulated together near the boundaries of coarser grains, subgrain structure formed in the matrix, as shown in Fig. 5b. The improvement of dislocation was impeded, and the dislocation piled up around the secondary phase

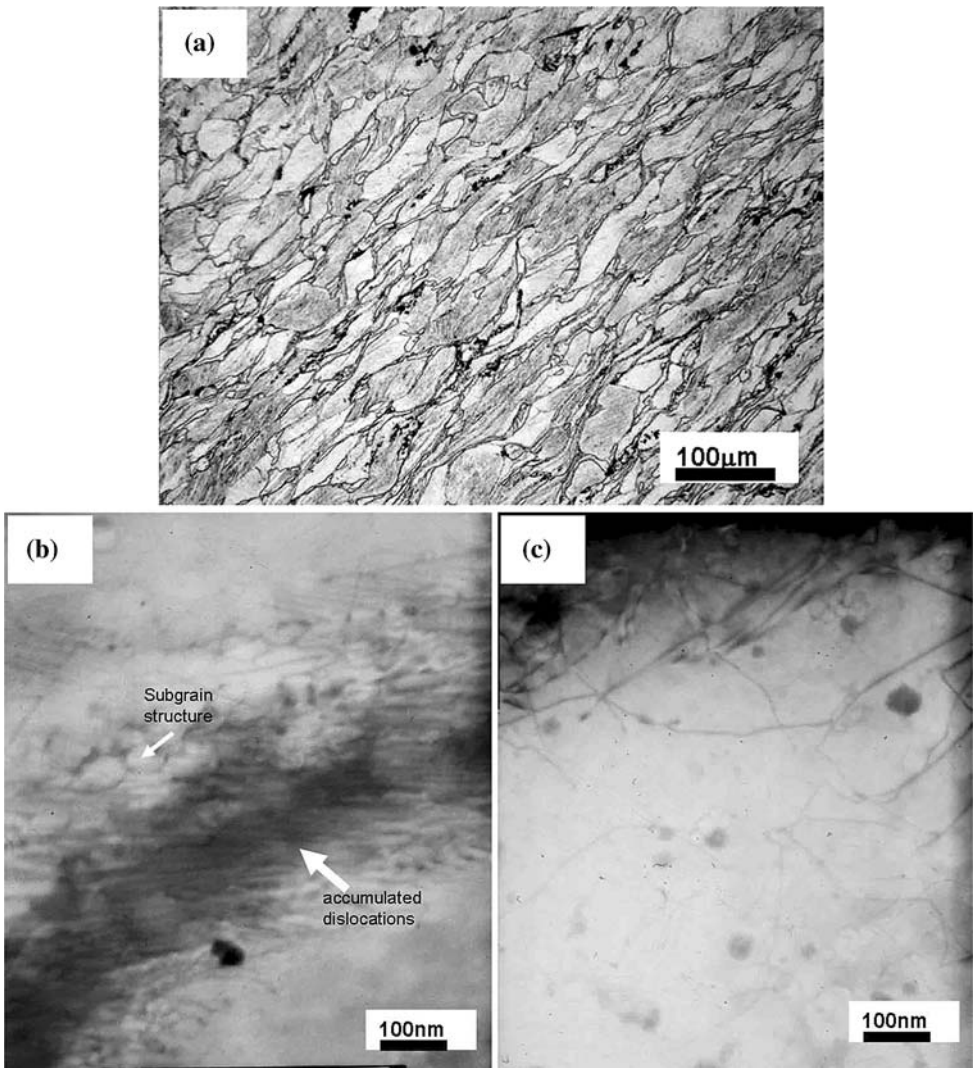

Fig. 5 Images of deformation specimens of alloy B: **a** OM image; **b** high density of dislocation and subgrain structure; **c** dislocations around secondary phase particles

particles which were located at grain boundaries or matrix (see Fig. 5c).

Figure 6 shows the XRD patterns of the as-extruded alloys. The figure shows that the phase constituents present in the as-extruded alloys include α-Mg solid solution, $Mg_{24}(Y, Gd)_5$, $Mg_5(Y, Gd)$, and $Mg_{12}Zn(Y, Gd)$ secondary phases. Compared with the as-cast alloys, it can be observed that no new phases are detected within the sensitivity limits of XRD.

Aging behaviors of extruded alloys and microstructures of peak-aged alloys

Figure 7 shows the age hardening behaviors of the as-extruded alloys A, B, C, and D at 220 °C and the standard deviation is given in parenthesis following the value of peak hardness. It can be seen that all the investigated alloys exhibit hardening response. The as-extruded specimens of alloy A displayed a distinct hardening effect at 24 h, and then reached a peak hardness of 116 (3.2) VHN after 120 h. The age hardening curve of as-extruded alloy B exhibits the best aging hardening response of all four alloys. It was found that the as-extruded alloy B exhibits an obvious hardening response at the beginning after 25 h, with a peak hardness of 119 (4.1) VHN being obtained at 122 h. Alloys C and D, both with large Zn additions, do not have an obvious increase in the hardness until 70 and 60 h, respectively. The as-extruded alloy C obtains a peak hardness of 99 (4.3) VHN after 118 h. The as-extruded alloy D reaches a peak hardness of 92 (3.4) VHN after 60 h. In other words, the addition of Zn between 0.5 and 1.5 wt.% to Mg–Y–Gd-based alloys results in a significant enhancement of the age hardening response at 220 °C.

In order to investigate the precipitation morphologies and discuss the reasons for the aging response at 220 °C, the TEM images and corresponding selected area electron diffraction (SAED) patterns from alloys B and D are shown in Fig. 8. In the peak-aged condition, i.e., 122 h, a great

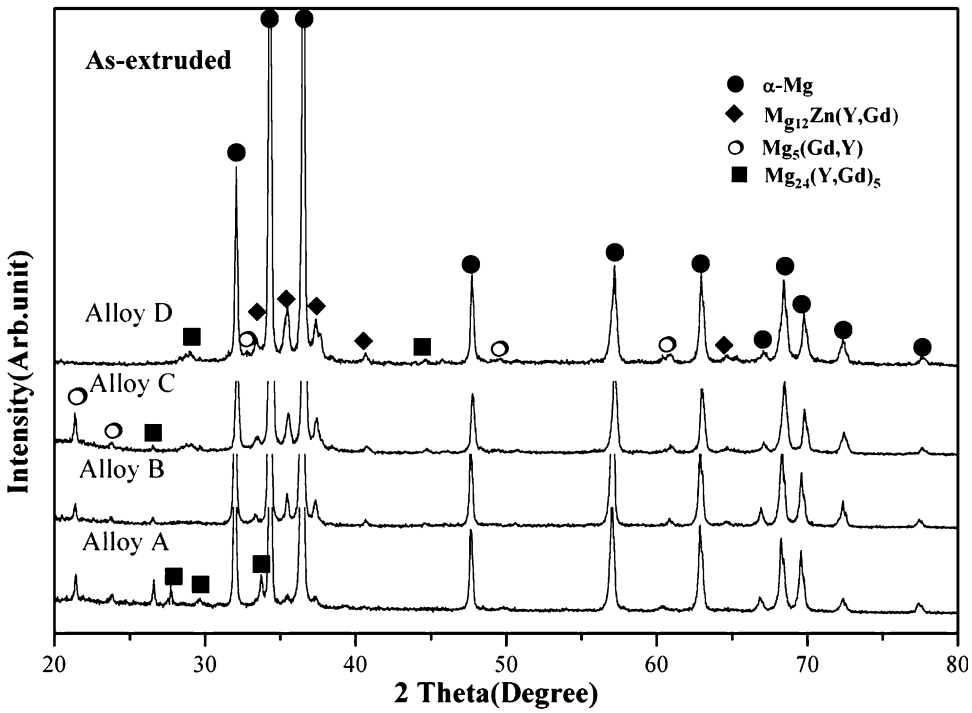

Fig. 6 XRD patterns of the as-extruded alloys A, B, C, and D

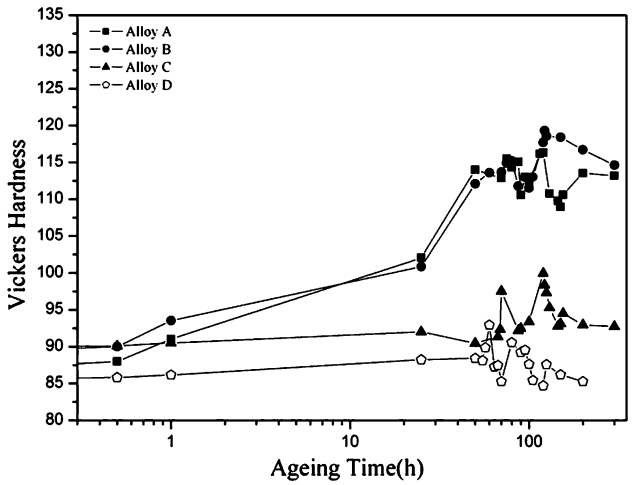

Fig. 7 Age hardening responses of the as-extruded alloys A, B, C, and D during aging at 220 °C

number of β' phase which are ellipsoidal in morphology were observed in peak-aged specimen of alloy B, as shown in Fig. 8a. The TEM observation of peak-aged specimen of alloy D shows that two types of phases coexist together throughout the α-Mg matrix. One is β' phase with an ellipsoidal morphology (see Fig. 8b) and the other is $MgZn_2$ phase distributed randomly in the matrix with a rod morphology [26], as shown in Fig. 8d. It is easy to find that amounts of β' phase in peak-aged specimen of alloy D is less than that in peak-aged specimen of alloy B.

The β' phase is the main secondary strengthening phase in all four alloys [27–30]. The TEM observation shows that the volume fraction of β' phase in alloy B is higher than that in alloy D. It has been reported that the volume fraction of this phase decreases with increasing Zn addition [31]. This leads to a less obvious age hardening response of the alloy with high Zn content, i.e., alloys C and D. As stated above, the addition of Zn between 0.5 and 1.5 wt.% has a great effect on the age hardening responses.

Mechanical properties of alloys

A comparison of the typical mechanical properties of all four alloys in different states is listed in Table 1. The strength and elongation of the as-cast alloys tend to improve with increasing the Zn addition, as seen in Table 1. Both as-cast alloys C and D have better mechanical properties than those of the alloys A and B. The results for alloy C show a better ultimate tensile strength (UTS) and tensile yield strength (YTS), the values are about 166 and 124 MPa, respectively, with an elongation of 7.6%. The values of UTS and YTS of alloy D are 164 and 130 MPa, respectively, and the elongation is 6.1%.

The mechanical properties are improved evidently after hot extrusion due to the refinement of the microstructure, as shown in Table 1, especially for the alloy C. The values of UTS and YTS of alloy C in as-extruded condition are about 356 and 242 MPa, respectively, with a good elongation of 8.9%. The UTS is improved by 190 MPa, and the increment of YTS is 118 MPa. The extrusion process is beneficial to improve the mechanical properties of alloys via microstructural refinement.

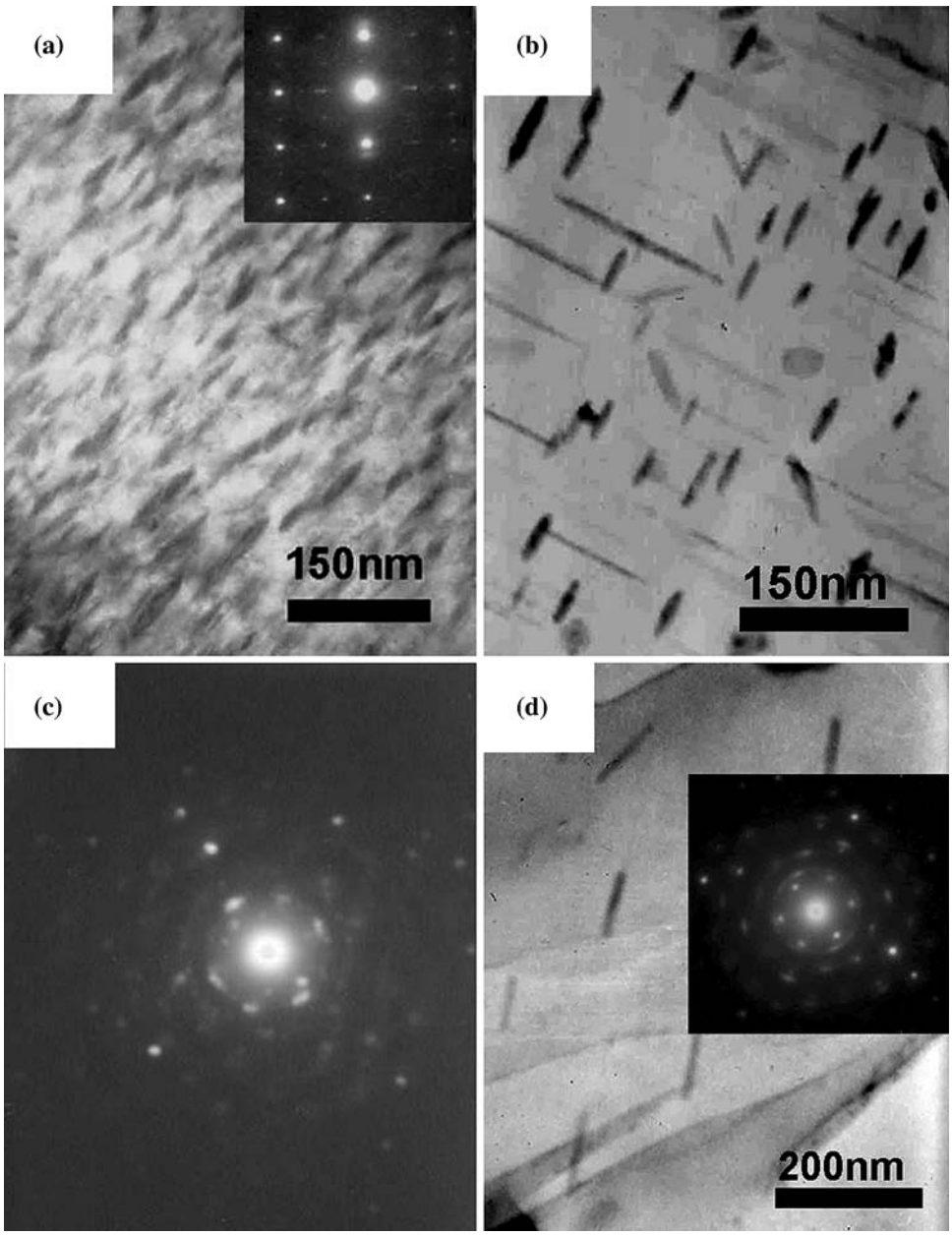

Fig. 8 TEM images and corresponding SAED patterns of peak-aged specimens: **a** β' phase in alloy B; **b** β' phase in alloy D; **c** SAED trace of β' in alloy D; **d** $MgZn_2$ phase in alloy D

However, when the Zn addition is more than 5%, such as alloy D in as-extruded or as-cast conditions, the mechanical properties except YTS decrease with further increasing Zn content (see Table 1), which is related to the large volume fraction of the LPS structure, as shown in Fig. 4g.

The tensile strength of the alloys A and B is greatly improved after peak aging. Both UTS and YTS of peak-aged alloy A are improved significantly, with values of 397 and 300 MPa, respectively. The peak-aged alloy B has the highest mechanical properties at room temperature, with UTS and YTS reaching 418 and 320 MPa, respectively, with an elongation of 6.2% (see Table 1). However, alloys C and D with high Zn content have less age hardening response. The values of the UTS and YTS of alloy D are 350 and 280 MPa, respectively.

Tensile properties of the peak-aged alloys at elevated temperature are shown in Fig. 9. The UTS and YTS of the peak-aged alloys decrease slowly with increasing temperature initially, as shown in Fig. 9a and b. The elongation increases gradually from room temperature to 200 °C. Further increasing the temperature up to 300 °C, the tensile strength values of all four alloys decrease rapidly, especially for alloy B. Meanwhile, the elongation of these alloys increases during hot deformation. The elongation of the alloy D has a highest value of 40.1% at 300 °C, whereas the elongation of the alloy A is lower.

Table 1 Tensile property of alloys A, B, C, and D at room temperature

Alloys	State	UTS (MPa)	YTS (MPa)	Elongation (%)
A	F	149 (2.1)	101 (3.2)	3.8 (0.7)
	As-extruded	320 (3.4)	214 (2.8)	7.1 (0.4)
	Peak-aged	397 (4.5)	300 (3.5)	5.7 (1.0)
B	F	159 (3.3)	110 (2.7)	4.2 (0.6)
	As-extruded	331 (2.7)	228 (3.2)	7.3 (0.5)
	Peak-aged	418 (3.8)	320 (4.2)	6.2 (0.3)
C	F	166 (2.7)	124 (3.1)	7.6 (0.5)
	As-extruded	356 (4.1)	242 (3.0)	8.9 (0.9)
	Peak-aged	359 (4.0)	296 (3.2)	7.1 (1.0)
D	F	164 (3.6)	130 (2.4)	6.1 (0.7)
	As-extruded	342 (4.1)	251 (4.2)	8.2 (0.5)
	Peak-aged	350 (2.1)	280 (3.7)	7.4 (0.8)

Note: standard deviation is given in parenthesis

As stated above, elongation of the alloys, in as-cast, as-extruded and peak-aged conditions increased with increasing Zn addition. Suzuki et al. [32] reported that addition of small amount of Y and Zn into a magnesium alloys decreases the stacking fault energy of these magnesium alloys. Furthermore, the Zn additions assist in the formation of LPS structures, leading to the minimum total energy in the system, which makes dislocations move on the energetically favored basal planes more readily [31]. This gives rise to a better elongation in the alloy which contains high content of Zn, companied with good tensile strength at elevated temperature.

Discussion

The solid solubility of Gd in magnesium is high (equilibrium solid solubility of 23.49 wt.% at 548 °C), but it declines quickly with decreasing temperature (equilibrium solid solubility of 3.82 wt.% at 200 °C), so it is considered to be an ideal system for precipitation hardening [7, 33]. As a result, more strengthening precipitates will form during peak aging at 220 °C.

However, the addition of Zn to the Mg–Y–Gd-based alloys leads to the formation of the LPS structure and the volume fraction of this phase increases with increasing Zn addition [31]. As a result, the content of RE (standing for Gd and Y) retained in the matrix decreased. Moreover, the Zn atom is smaller (0.13 nm), and the RE atoms are larger (both 0.18 nm) than the atomic radius of Mg (0.16 nm), and the Zn would like to substitute for RE in the supersaturated α-Mg matrix. When these alloys were aged at 220 °C, the volume fraction of β' phase decreased with increasing Zn addition.

Kawamura et al. [34] developed the highest strength magnesium alloy with yield strength of 600 MPa by using a rapid solidification powder metallurgy method. The 18R LPS morphology was observed in this alloy. Kawamura regarded the LPS morphology as the main strengthening phase. However, the content of RE in the supersaturated matrix decreased with Zn addition, and it led to a decreased volume fraction of the β' phase. So, the aging responses of these alloys decrease with increasing Zn addition.

As stated above, the improved mechanical properties of the alloy with Zn addition between 0.5 and 1.5 wt.% are

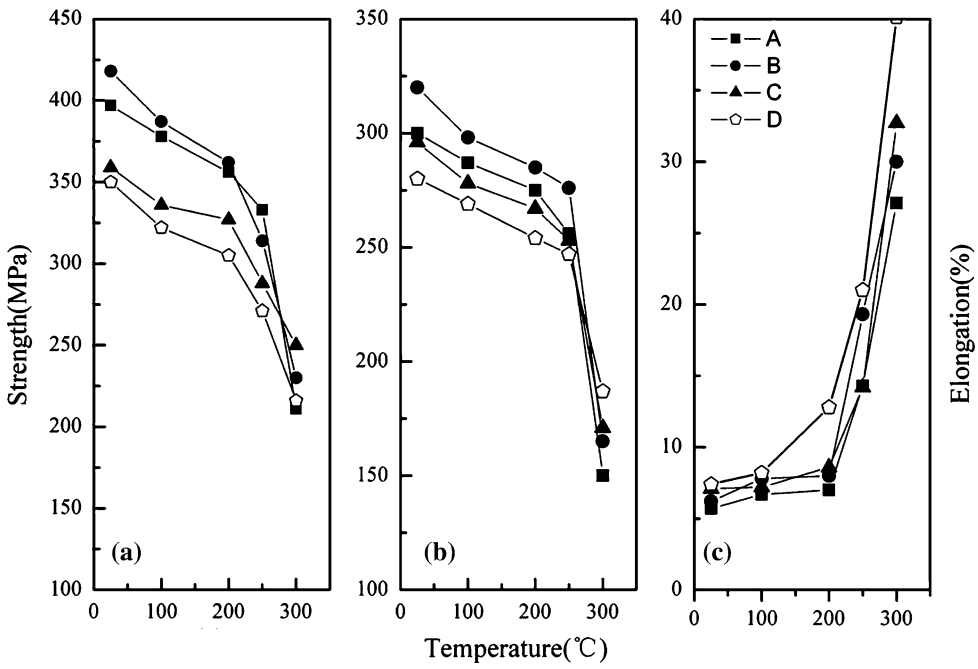

Fig. 9 Tensile properties of specimens of the peak-aged alloys A, B, C, and D as a function of temperatures: **a** UTS; **b** YTS; **c** the elongation

attributed to both the LPS and β' phases coexisting together.

Conclusions

In this article, the microstructures and the tensile properties of alloys A, B, C, and D have been investigated. The investigation can lead to the following conclusions:

1. Addition of Zn led to the formation of the LPS structure and the volume fraction of this phase increased with increasing the Zn addition.
2. Hot-extrusion processing had an obviously effect on microstructure refinement. DRX occurred during hot deformation and refined the microstructures.
3. The β' phase is the main secondary strengthening phase and precipitates within the matrix during aging at 220 °C. However, the volume fraction of this phase decreased with increasing Zn addition.
4. The peak-aged alloy B exhibited the highest peak hardness and tensile strength. The values of UTS and YTS are 418 and 320 MPa, respectively, at room temperature. The tensile strength of this alloy at 200 °C is still high, with good values of UTS and YTS, i.e., 362 and 285 MPa, respectively.

Acknowledgements This project was supported by Hi-Tech Research and Development Program of China (2006AA03Z520), Chinese Academy of Sciences and Jilin Province, and Baikov Institute of Metallurgy and Materials Science, Russian Academy of Sciences, Moscow.

References

1. Kojima Y, Aizawa T, Kamado S, Higashi K (2003) Mater Sci Forum 3:419
2. Polmear IJ (1994) Mater Sci Technol 10:1
3. Anyanwu IA, Kamado S, Kojima Y (2001) Mater Trans JIM 42:1206
4. Anyanwu IA, Kamado S, Kojima Y (2001) Mater Trans JIM 42:1212
5. Wei LY, Dunlop GL, Westengen H (1995) Metall Mater Trans A 26:1705
6. Clark JB (1965) Acta Metall 13:1281
7. Nie JF, Gao X, Zhu SM (2005) Scr Mater 53:1049
8. Balasubramani N, Pillai UTS, Pai BC (2008) J Alloys Compd 460:1
9. Yamasaki M, Anan T, Yoshimoto S, Kawamura Y (2005) Scr Mater 53:799
10. Vostry P, Smola B, Stulikova I, Buch FV, Mordike BL (1999) Phys Status Solidi A 175:491
11. Smola B, Stulikova I, Buch FV, Mordike BL (2002) Mater Sci Eng A 324:113
12. Apps PJ, Karimzadeh H, King JF, Lorimer GW (2003) Scr Mater 48:1023
13. Gao X, He SM, Zeng XQ, Peng LM, Ding WJ, Nie JF (2006) Mater Sci Eng A 431:322
14. Kawabata T, Matsuda K, Kamado S, Kojima Y, Ikeno S (2003) Mater Sci Forum 303:419
15. Yamada K, Ohkubo Y, Shiono M, Watanabe H, Kamado S, Kojima Y (2006) Mater Trans JIM 47:1066
16. Padezhnova EM, Melnik EV, Miliyevskiy RA, Dobatkina TV, Kinzhibalo VV (1982) Russ Metall (Metally) (Engl Transl) 4:185
17. Luo ZP (2000) J Mater Sci Lett 19:813
18. Zhang M, Zhu SJ, Chen GL, Zhang BF, Guan SK (2005) Found Tech 26:983
19. Liu JY, Zhang ZZ, Hua M, Ma LQ, Shen XD (2006) Found Tech 27:258
20. Yoshimoto S, Yamasaki M, Kawamura Y (2006) Mater Trans 47:959
21. Itoi T, Seimiya T, Kawamura Y, Hirohashi M (2004) Scr Mater 51:107
22. Poter DA, Eastering KE (1992) Phase transformations in metals and alloys. Chapman & Hall, London
23. Mohri T, Mabuchi M, Nakamura N, Asahina T, Iwasaki H, Aizawa T, Higashi K (2000) Mater Sci Eng A 290:139
24. Yang Z, Guo YC, Li JP, He F, Xia F, Liang MX (2008) Mater Sci Eng A 485:487
25. Tan JC, Tan MJ (2003) Mater Sci Eng A 339:124
26. Kim IJ, Bae DH, Kim DH (2003) Mater Sci Eng A 339:313
27. He SM, Zeng XQ, Peng LM, Gao X, Nie JF, Ding WJ (2006) J Alloys Compd 421:309
28. Lin L, Chen LJ, Liu Z (2008) J Mater Sci 43:4493. doi: 10.1007/s10853-008-2650-x
29. Peng QM, Dong HW, Wang LD, Wu YM, Wang LM (2007) J Mater Sci 42:3908. doi:10.1007/s10853-006-0451-7
30. Aghion E, Gueta Y, Moscovitch N (2008) J Mater Sci 43:4870. doi:10.1007/s10853-008-2708-9
31. Honma T, Ohkubo T, Kamado S, Hono K (2007) Acta Mater 55:4137
32. Suzuki M, Kimura T, Koike J, Maruyama K (2003) Scr Mater 48:997
33. Lu YZ, Wang QD, Zeng XQ, Ding WJ, Zhai WQ, Zhu YP (2000) Mater Sci Eng A 278:66
34. Kawamura Y, Hayashi K, Inoue A, Masumoto T (2001) Mater Trans JIM 42:1172